LIMNOLOGY
and
OCEANOGRAPHY

ASLO

Limnol. Oceanogr. 63, 2018, 2579–2594

doi: 10.1002/lno.10961

Large Phaeodaria in the twilight zone: Their role in the carbon cycle

Michael R. Stukel,[1,2*] **Tristan Biard**,[3] **Jeffrey Krause**,[4] **Mark D. Ohman**[3]

[1]Department of Earth, Ocean, and Atmospheric Science, Florida State University, Tallahassee, Florida
[2]Center for Ocean-Atmospheric Prediction Studies, Florida State University, Tallahassee, Florida
[3]Scripps Institution of Oceanography, University of California San Diego, San Diego, California
[4]Dauphin Island Sea Lab, University of South Alabama, Dauphin Island, Alabama

Abstract

Advances in in situ imaging allow enumeration of abundant populations of large Rhizarians that compose a substantial proportion of total mesozooplankton biovolume. Using a quasi-Lagrangian sampling scheme, we quantified the abundance, vertical distributions, and sinking-related mortality of Aulosphaeridae, an abundant family of Phaeodaria in the California Current Ecosystem. Inter-cruise variability was high, with average concentrations at the depth of maximum abundance ranging from < 10 to > 300 cells m^{-3}, with seasonal and interannual variability associated with temperature-preferences and regional shoaling of the 10°C isotherm. Vertical profiles showed that these organisms were consistently most abundant at 100–150 m depth. Average turnover times with respect to sinking were 4.7–10.9 d, equating to minimum in situ population growth rates of ~ 0.1–0.2 d^{-1}. Using simultaneous measurements of sinking organic carbon, we find that these organisms could only meet their carbon demand if their carbon : volume ratio were ~ 1 μg C mm^{-3}. This value is substantially lower than previously used in global estimates of rhizarian biomass, but is reasonable for organisms that use large siliceous tests to inflate their cross-sectional area without a concomitant increase in biomass. We found that Aulosphaeridae alone can intercept > 20% of sinking particles produced in the euphotic zone before these particles reach a depth of 300 m. Our results suggest that the local (and likely global) carbon biomass of Aulosphaeridae, and probably the large Rhizaria overall, needs to be revised downwards, but that these organisms nevertheless play a major role in carbon flux attenuation in the twilight zone.

The biological pump transports organic carbon produced by photosynthesis in the ocean's euphotic zone to deeper depths (Silver and Gowing 1991; Ducklow et al. 2001; Boyd and Trull 2007; Honjo et al. 2008). In the process, it sequesters carbon dioxide from the atmosphere and supplies food to the deep-water column and benthos. The efficiency of carbon transport to the seafloor and the duration that this carbon will be sequestered from the surface ocean and atmosphere are determined by remineralization processes in the deep epipelagic and mesopelagic zone—together referred to as the ocean's "twilight zone" (Buesseler et al. 2007; Buesseler and Boyd 2009; Kwon et al. 2009). This layer supports a diverse community of organisms from microbes to nekton that are typically food-limited (Steinberg et al. 2008*b*; Robinson et al. 2010). Organic matter is delivered to these communities by slowly settling particles, active transport mediated by vertically migrating metazoans, and diffusive and advective flux of detritus and dissolved organic molecules (Carlson et al. 1994; Ducklow et al. 2001; Steinberg and Landry 2017).

*Correspondence: mstukel@fsu.edu

Additional Supporting Information may be found in the online version of this article.

Large Rhizaria (> 600-μm; including polycystine Radiolaria, Phaeodaria, Foraminifera, and Acantharia) are frequent residents of the twilight zone (Boltovskoy et al. 2010; Biard et al. 2016). However, they are seldom included in mesopelagic carbon budgets for multiple reasons: They are seldom preserved quantitatively in net tows used to collect mesozooplankton and are difficult to culture (Suzuki and Not 2015). They also do not fit well within typical plankton classifications, because although they are protists (i.e., unicellular eukaryotes), their size is more similar to common metazoan organisms, and many are mixotrophic (Caron et al. 2012). Nevertheless, the development of in situ optical instruments has shown that they are abundant throughout the world ocean and often comprise close to half of total mesozooplankton biovolume in oligotrophic regions (Biard et al. 2016). It is thus clear that the ecological and biogeochemical importance of these organisms deserves more thorough examination.

Previous studies have shown that rhizarians are often contributors to export flux, as evidenced by their frequent presence in sediment trap samples (Takahashi and Honjo 1981; Michaels et al. 1995; Steinberg et al. 2008*a*; Lampitt et al. 2009; Ikenoue et al. 2015). This is not surprising, since

foraminifera, acantharians, and radiolarians all have mineralized tests (constructed of calcium carbonate, strontium sulfate, and opaline silica, respectively). However, the abundance of silicified taxa is likely under-estimated in long-term, moored sediment trap collections due to rapid remineralization of these organisms (Gowing and Coale 1989), especially over multi-month deployments. These silicified taxa were previously grouped together taxonomically into the Radiolaria, although genetic evidence has now shown that the Radiolaria are not monophyletic, and that phaeodarians should be grouped within the Cercozoa, while polycystine radiolarians are more closely related to Acantharia and Foraminifera (Polet et al. 2004).

Within the California Current Ecosystem (CCE) it has been suggested that large rhizarians (primarily phaeodarians) comprise over 50% of total mesozooplankton biomass (Biard et al. 2016). These organisms thus deserve special attention. Phaeodarians have a large silica test (referred to as a scleracoma) that can range in size from several hundred micrometers to several millimeters. A substantially smaller central region is composed of the central capsule that contains the endoplasm and nuclei, and a phaeodium, often attached to the central capsule, believed to be comprised of food vacuoles and waste particles (Nakamura and Suzuki 2015; Nakamura et al. 2015). In the CCE, Phaeodaria are predominantly found in the 100–150 m depth range (Ohman et al. 2012; Biard et al. 2018, as "Radiolaria"). These subsurface taxa are likely to be flux feeders that were reported to feed predominantly on sinking material, although protists and bacteria are also found in their phaeodium (Gowing 1986, 1989; Gowing and Wishner 1992; Gowing and Bentham 1994). In a companion study to the present work, results from paired measurements of phaeodarian abundance and vertical flux made during quasi-Lagrangian experiments were used to quantify the role of Phaeodaria in the regional silica cycle and to infer their role in global silica export (Biard et al. 2018). In this study, we use these same abundance and flux data to assess the turnover time of these organisms and the corresponding growth rates necessary to support sinking loss. Based on these growth rates, we can assess the carbon demand (CD) of these twilight zone organisms, which we then compare to carbon supply estimated from vertical carbon flux measurements and the abundance of protists beneath the euphotic zone in the CCE. We find that carbon supply only meets CD if we assume substantially lower carbon : biovolume ratios than were utilized to make global estimates of rhizarian biomass (Biard et al. 2016). Despite these reduced biomass estimates, we find that Phaeodaria can have important roles in mesopelagic flux attenuation during periods when they are present in high abundances.

Methods

In situ sampling

Our results are derived from five cruises of the CCE-LTER Program (Fig. 1). Cruise plans and detailed regional characteristics are described in other papers and we mention them briefly here: On P0810 (October 2010), we sampled conditions ranging from mild upwelling near Point Conception to oligotrophic conditions offshore (Landry et al. 2012). The P1106 cruise (June 2011) focused on a gradient region south and slightly west of Point Conception (Krause et al. 2015). The P1208 (August 2012) cruise investigated a strong and stable front separating cyclonic and anti-cyclonic eddies west of Point Conception (Stukel et al. 2017). On P1408 (August 2014), we sampled during a northeast Pacific-wide warm anomaly that depressed upwelling in the region, leading to abnormally warm, stratified, low-productivity conditions throughout the region (Morrow et al., unpubl.; Nickels and Ohman, 2018). The P1604 (April 2016) cruise sampled a wide range of ecosystem conditions near the end of the 2015–2016 El Niño (Morrow et al., unpubl.; Nickels and Ohman, 2018).

On all cruises, our experimental design was focused on 2- to 5-d quasi-Lagrangian experiments ("cycles") during which we followed water parcels using in situ drifting arrays with Iridium-enabled surface floats and 1-m diameter × 3-m long holey sock drogues centered at a depth of 15 m (Landry et al. 2009). Two arrays were deployed simultaneously. One array was used for in situ growth and protistan grazing experiments (Landry et al. 2009). The second array was a platform for deployment of sediment traps (Stukel et al. 2013). Our Lagrangian sampling scheme allowed for co-ordinated rate and biomass measurements within a coherent oceanographic feature as it evolved over a short period of time. Standard measurements made daily on each water parcel included: day-night paired oblique net tows for mesozooplankton abundance and biomass (Ohman et al. 2012); CTD casts with attached Niskin rosette for bacteria and protist biomass and nutrient measurements (Taylor et al. 2012); primary productivity measured daily in situ at 6–8 depths by $H^{14}CO_3^-$ uptake (Morrow et al., unpubl.), and ^{238}U-^{234}Th disequilibrium to validate sediment trap collection efficiency (Stukel et al. 2011).

Sinking particles were collected using surface-tethered VERTEX-style sediment traps (Knauer et al. 1979). Trap tubes were acrylic cylinders with 8 : 1 (height : diameter) aspect ratios and a baffle consisting of 13 smaller tapered tubes with similar 8 : 1 aspect ratios (Stukel et al. 2013). We deployed 8–12 tubes per depth. On P0810, P1106, and P1208 traps were deployed at 100 m depth and near the base of the euphotic zone (if the euphotic zone was shallower than 70 m). On P1408 and P1604, an additional set of traps was placed at 150 m. Tubes were deployed with a salt-water brine comprised of 0.1-μm filtered seawater, amended with 50 g L^{-1} NaCl and 0.4% formaldehyde (final concentration). After recovery, the density interface separating the brine from overlying seawater was determined for each tube and the overlying seawater was removed by gentle suction. The tubes were then filtered through a 200-μm Nitex filter, which was examined under a stereomicroscope to allow removal of swimming

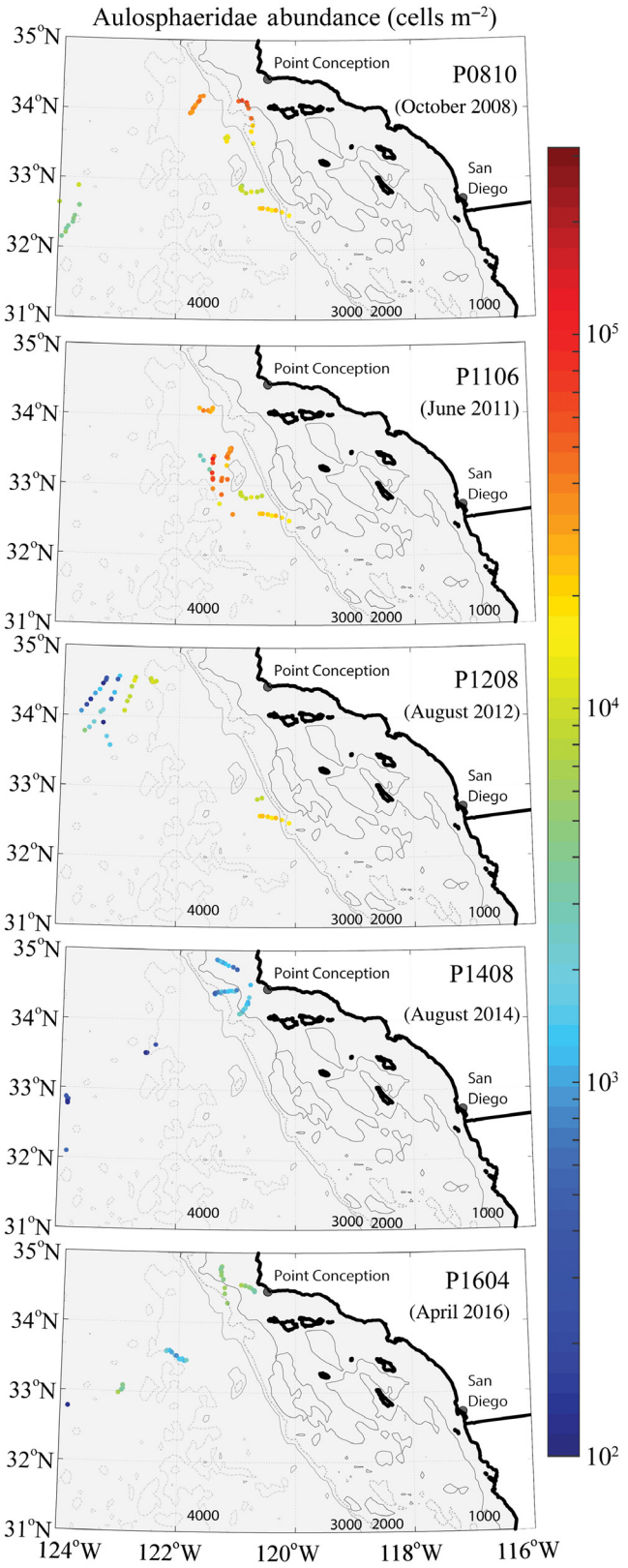

Fig. 1. Aulosphaeridae vertically integrated abundance (cells m^{-2}) measured by UVP5 on individual CTD casts on each of our cruises. Contour lines are bathymetry (m).

mesozooplankton and quantification of large Rhizaria (see below). The contents (excluding swimmers) of the > 200-μm filters were then rinsed back into the samples, which were split using a Folsom splitter for a variety of analyses including C/N, ^{234}Th, and microscopic analysis of fecal pellets. Comparison of ^{234}Th flux into the sediment traps with estimates of ^{234}Th flux made from ^{238}U-^{234}Th disequilibrium measurements and a one-dimensional steady-state model suggested no collection bias for the sediment traps (Stukel et al. 2015; Morrow et al., unpubl.). For more details, see Stukel et al. (2013) and Morrow et al. (unpubl.).

Rhizarian measurements

Large rhizarians were quantified in situ using the Underwater Vision Profiler (UVP5, Picheral et al. 2010; Biard et al. 2016). The UVP5 is a camera system that can be mounted on a CTD-Niskin rosette to image plankton and other particles. Its resolution is sufficient to identify organisms with equivalent spherical diameter (ESD) greater than 600-μm. The UVP5 was mounted downward facing on the bottom of the rosette and only used as the rosette descended (with typical descent speeds of 0.5 m s^{-1} within 100 m of the surface and 1 m s^{-1} at deeper depths). The UVP5 samples 0.5–1.0 L per image. Typical sample volumes on our deployments were 10 L m^{-1}. Data used in this manuscript come from 242 independent casts made on 25 different Lagrangian cycles. ZooProcess software (Gorsky et al. 2010) was used for image analysis. Briefly, vignettes were automatically extracted from images and classified into taxonomic groups. Rhizarian groups included Phaeodaria (further subdivided to family level), Collodaria, Acantharia, and Foraminifera. However, for this study, only vignettes corresponding to the most abundant Phaeodarian family in the dataset (Aulosphaeridae) were utilized (a total of 25,185 vignettes). Morphometric data (including ESD) were then assigned for each vignette and the taxonomic assignment of each vignette was manually confirmed. For more details, see Biard et al. (2016, 2018).

We also quantified Rhizaria vertical flux into sediment traps. The abundance of > 200-μm Rhizaria was determined by manual counting of rhizarian cells retained on 200-μm Nitex filters used for removing swimming mesozooplankton (many smaller rhizarians passed through this mesh size and hence were not quantified). These analyses were done at sea, typically within 24 h of sediment trap recovery to prevent dissolution or mechanical destruction of delicate tests during storage and/or transport. Starting with the P1106 cruise, we consistently counted the abundance of Castanellidae and Aulosphaeridae (5–12 replicates per depth for each deployment). Smaller rhizarians were also noticed, but not consistently enumerated, because they likely were not quantitatively retained on the 200-μm filter. Although Castanellidae were found in the sediment traps at similar abundances as Aulosphaeridae they were not quantified by the UVP5 because their size (400–900 μm ESD) was too small to be reliably identified in UVP5 images. At least two morphotypes of Aulosphaeridae were noted in the sediment trap based on the different geometric patterns in their siliceous tests. We group both

morphotypes together for analyses. Often we identified Aulosphaeridae tests in the sediment traps without obvious cytoplasm associated with them. These were counted with intact cells, because we believe them to reflect the remains of dead Aulosphaeridae and hence include them in subsequent mortality estimates. We measured the ESD of 15 Aulosphaeridae cells collected in the sediment trap (randomly chosen from samples spanning all cruises) using a stereomicroscope with attached digital camera and Image J software.

Aulosphaeridae vital rate calculations

Because of their large size and Si tests, sinking is an important (potentially dominant) loss term for Aulosphaeridae in the water column (although it is important to note that sinking of Aulosphaeridae tests may follow mortality due to other causes). If we assume no shallow remineralization of their rapidly sinking tests, we can calculate the turnover time (τ) by dividing their vertically integrated standing stock by their sinking flux as measured by sediment traps. Specific growth rates at steady state can then be calculated as $1/\tau$.

We can also calculate the CD of an individual cell from τ if we know the carbon content of the cell. To our knowledge, only one study has directly measured carbon : volume (C : V) ratios of large Rhizaria and the results showed widely varying C densities (Michaels et al. 1995). Mixed Acantharia had a C : V ratio of 2.6 μg C mm^{-3}, while Foraminifera ranged from 18 μg C mm^{-3} to 180 μg C mm^{-3} and solitary Radiolaria (Collodaria) ranged from 9 μg C mm^{-3} to 280 μg C mm^{-3}. However, it is important to note that Michaels et al. (1995) defined the volume by the test size for Foraminifera and by the central capsule size for Radiolaria, while the pseudopodial network extended over a much greater volume. The C : V ratio of the entire organism (including the ectoplasm) would be substantially lower. Biard et al. (2016) assumed a value of 80 μg C mm^{-3} for phaeodarians. This conversion for protistan microzooplankton was based on arguments advanced by Beers and Stewart (1970) that specific gravity = 1.0, water content = 80% of wet weight, and carbon is 40% of the dry weight (i.e., similar carbon : volume ratios as typical crustaceans). This estimate for protists is similar to that which would be derived from the allometric relationships developed by Menden-Deuer and Lessard (2000): $B = 0.216 \times V^{0.939}$, where B is the carbon biomass in units of pg C and V is the biovolume in units of μm^3. This equation would suggest a C : V ratio of 56 μg C mm^{-3} for a 2-mm diameter cell. However, Menden-Deuer and Lessard (2000) caution that their relationship should not be used for Foraminifera, Radiolaria, Acantharia, and Phaeodaria (collectively referred to in the paper as "sarcodines"). Many rhizarians, including Aulosphaeridae, are likely less carbon-dense and more gelatinous than other protists. Instead of assuming that an Aulosphaeridae cell has a C : V ratio throughout its entire scleracoma that is similar to the carbon density of a nanoplanktonic or microplanktonic protist, we can consider what the C : V ratio would be if the carbon were concentrated within the central capsule of the cell (Fig. 2a,b). From UVP5 images, we calculated that the central capsule (including the phaeodium, if present, as we could not distinguish the two from UVP5 images) comprised ~ 1.6% of the volume of the scleracoma (i.e., the central capsule diameter : scleracoma diameter was 1 : 4). A 2-mm Aulosphaeridae cell would therefore have a central capsule volume of 0.065 mm^3 and a carbon biomass of 4.8 μg C (based on the allometric relationship of Menden-Deuer and Lessard 2000). Divided by the volume of the scleracoma, this yields a total carbon density of 1.1 μg C mm^{-3}. In the results section, we use this lower C : V ratio, because we found that with the C : V ratio of 80 μg C mm^{-3} used by Biard et al. (2016) carbon supply to Aulosphaeridae cells was ~ 2 orders of magnitude too low to meet their demand (*see* "The ecological role of Aulosphaeridae" section).

Using this C : V ratio, we can calculate CD as equal to the carbon biomass divided by the gross growth efficiency and the turnover time:

$$\mathrm{CD} = \mathrm{CV} \times \frac{\pi \, \mathrm{ESD_{cell}}^3}{6 \, \mathrm{GGE} \times \tau} \quad (1)$$

where CD is in units of μg C cell^{-1} d^{-1}, CV is in units of μg C mm^{-3}, $\mathrm{ESD_{cell}}$ is in units of mm, and GGE is the gross growth efficiency of Aulosphaeridae. We will assume that Aulosphaeridae living in the twilight zone minimize their energy expenditures and hence have GGE = 0.4, which is on the high end of the range for protists (Straile 1997).

Since Aulosphaeridae do not have algal symbionts and show biomass peaks slightly below the euphotic zone, we surmise that they are predominantly flux feeders (Gowing 1989; Nöthig and Gowing 1991). We can calculate carbon supply to Aulosphaeridae based on passive flux feeding ($\mathrm{CS_{FF}}$) as the effective cross-sectional area of the cell multiplied by the sinking carbon flux:

$$\mathrm{CS_{FF}} = F \times \frac{\pi}{4} \times 10^{-6} \times \mathrm{ESD_{eff}}^2 \quad (2)$$

where F is sinking carbon flux in units of μg C m^{-2} d^{-1}, CS is in units of μg C cell^{-1} d^{-1}, and $\mathrm{ESD_{eff}}$ is the effective ESD of the area over which it can intercept particles (units of mm). $\mathrm{ESD_{eff}}$ depends on both the cross-sectional area of the Aulosphaeridae cell and the effective diameter of sinking particles (D_{par}), which are primarily mesozooplankton fecal pellets in the CCE (Stukel et al. 2013; Morrow et al., unpubl.). $\mathrm{ESD_{eff}}$ also depends on the length of the narrow siliceous spines that extend radially from its siliceous sphere, increasing the effective capture radius by ~ 25% (Fig. 2). With these assumptions, we find that $\mathrm{ESD_{eff}}$ is equal to $1.25 \times \mathrm{ESD_{cell}} + D_{\mathrm{par}}$ (*see* Eq. A1 in the Supporting Information Appendix).

Aulosphaeridae also potentially consume carbon through passive flux feeding on swimming protists. These prey would be delivered by the random walk movement of motile prey. This

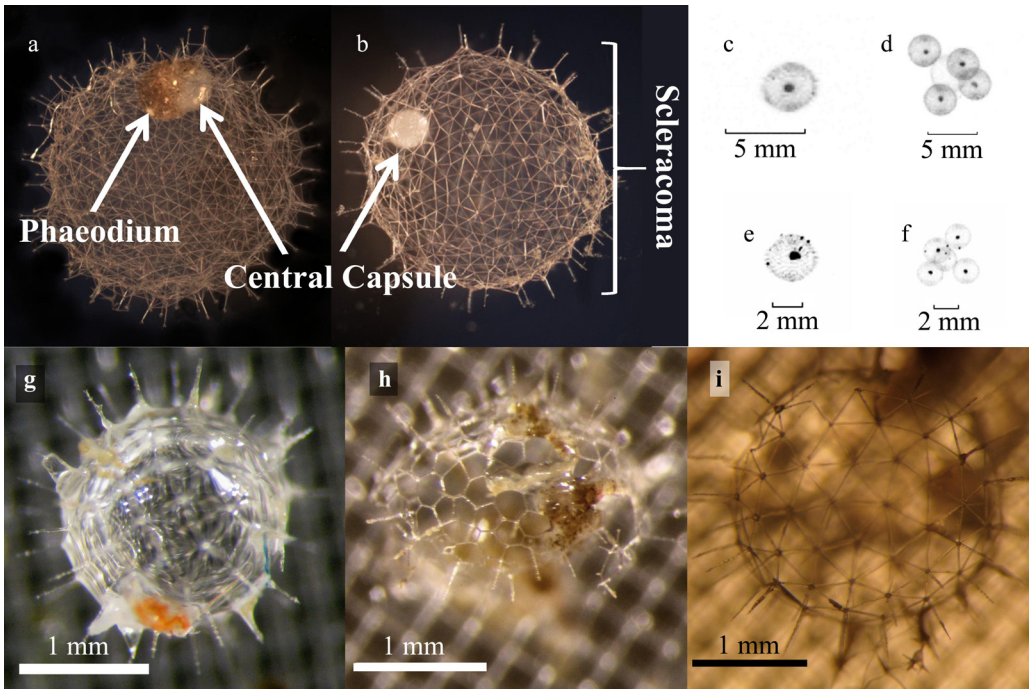

Fig. 2. Aulosphaeridae images. (**a**, **b**) High-resolution images of net-caught Aulosphaeridae with and without visible phaeodium. (**c**–**f**) UVP5 images. (**g**–**i**) Aulosphaeridae collected in sediment trap.

food supply (CS_{RW}) can be determined from Supporting Information Eq. A2 if we assume reasonable estimates for protistan swimming speeds and measure protistan biomass (*see* Supporting Information Appendix). We find that for a 2-mm Aulosphaeridae cell, $CS_{RW} = 4 \times 10^{-5} \times C_{pro}$, where C_{Pro} is in units of μg C m^{-3} and CS_{RW} is in units of μg C d^{-1}. Rhizaria also consume heterotrophic bacteria. However, since bacterial swimming speeds are typically 20–60 μm s^{-1} (Kiorboe et al. 2002) and bacterial biomass is typically ~ 3 μg C L^{-1} in the 100–150 m depth range in the CCE (Samo et al. 2012; Landry and California Current Ecosystem 2017), bacterial carbon supply to Aulosphaeridae is likely negligible and we do not include it in subsequent calculations.

To determine the role of Aulosphaeridae in the remineralization of sinking particles produced in the euphotic zone, we consider the cross-sectional area of the community at any given depth. This can be calculated from the product of the area of an individual cell (as determined by ESD_{eff} above) and the abundance of Aulosphaeridae over any given depth range. The fraction of particles produced in the surface layer that are intercepted by Aulosphaeridae as a function of depth can then be calculated as: $PerInt(d) = Sink(d)/Sink(d_0)$, where $Sink(d_0)$ is the flux from an arbitrary depth taken to be the start of the twilight zone. $Sink(d)$ is calculated by assuming that $Sink(d)$ is equal to flux at an incrementally shallower depth ($Sink(d - \Delta d)$ multiplied by one minus the fraction of the water column occluded by Aulosphaeridae living in the depth range from $d - \Delta d$ to d:

$$Sink(d) = Sink(d-\Delta d) \times \left(1 - A_{Aul}(d) \times \frac{\pi}{4}(ESD_{eff}(d))^2 \times 10^{-6}\right) \quad (3)$$

where $A_{Aul}(d)$ is the abundance of Aulosphaeridae in the depth range from d to $d + \Delta d$. We iterated Eq. 5 with depth to calculate $PerInt(d)$ with a vertical resolution of 1 m. The effective remineralization rate constant for particles produced in the euphotic zone and intercepted by Aulosphaeridae can be calculated as $\lambda_{Aul} = -\ln(Sink(d_0)/Sink(d_x))/(d_x - d_0)$. To compare to sediment trap-determined total remineralization rate constants, we used values of $d_0 = 50$ m and $d_x = 150$ m. We quantify the total carbon remineralization length constant from sediment trap measurements using the equation: $\lambda_{tot} = -\ln(Flux(d_0)/Flux(d_y))/(d_y - d_0)$, where $Flux(d_0)$ and $Flux(d_y)$ are carbon flux into sediment traps at depths of d_0 and d_y. We note that λ_{Aul} quantifies the role of Aulosphaeridae in intercepting (and consuming) sinking particles produced in the euphotic zone, but not their role in total carbon remineralization because not all organic carbon intercepted by Aulosphaeridae is respired (some contributes to deeper flux as sinking Aulosphaeridae cells and/or sinking egesta produced by Aulosphaeridae).

Results

Cruise conditions and Aulosphaeridae abundance

Our experimental plan utilized the inherent spatial, seasonal, and interannual variability in the CCE region to sample across a wide range of ecosystem conditions. Cruise P0810 occurred in October which is typically a quiescent month in the CCE. However, early in the cruise upwelling-favorable winds blew from the north, driving upwelling that influenced cycles 0810-3 to 0810-6. Surface Chl and primary productivity

were lowest on cycles 0810-2 (0.20 μg Chl *a* L^{-1} and 10.3 μg C L^{-1} d^{-1}), which was furthest from shore, and 0810-6 (0.22 μg Chl *a* L^{-1} and 7.5 μg C L^{-1} d^{-1}), which was on the offshore side of a strong frontal gradient. Cycle 0810-5 was conducted on the coastal side of the same frontal gradient and was the most productive water parcel sampled on the cruise (1.47 μg Chl *a* L^{-1} and 113 μg C L^{-1} d^{-1}at the surface). Aulosphaeridae abundance (determined in situ by UVP5) was high and variable on P0810, with maximum concentrations reached on Cycles 0810-1 and 0810-3 (Fig. 1; Table 1, Supporting Information Table S1), which were both characterized by moderate productivity and phytoplankton biomass. On these cycles, Aulosphaeridae reached maximum abundances of 300–600 cells m^{-3} at depths of ~ 100 m (Fig. 3). On the four other cycles, maximum abundances peaked in the range of ~ 40–100 cells m^{-3}.

The P1106 cruise featured the highest Aulosphaeridae abundances. With the exception of Cycle 1106-2, all the cycles on the cruise reached maximum cell abundances of > 340 cells m^{-3} at depths between 100 m and 150 m. The low abundances on Cycle 1106-2 were paired with low Chl and NO_3^-, although Chl and NO_3^- were similarly low on 1106-5, which had high Aulosphaeridae abundance. Both of these cycles were on the oceanic side of a gradient region. The other four cycles had elevated nutrients, phytoplankton, and productivity and were in the middle (1106-1 and 1106-6) or on the coastal side (1106-3 and 1106-4) of the gradient region.

Cycles on P1208 were conducted either within or in the water to either side of a strong, stable front separating two eddies. Aulosphaeridae abundances were substantially higher in cycles on the coastal side or in the core of the front (1208-3 and 1208-1, respectively; peak concentrations of 100–150 cells m^{-3}) than in cycles that were on the offshore side of the front where frontal expression was subsurface (1106-2 and 1106-5; peak of 10–15 cells m^{-3}) or the offshore region (< 3 cells m^{-3}).

The P1408 cruise occurred during strong warm water anomalies in the Northeast Pacific that led to elevated temperatures, decreased upwelling, and reduced nutrient and phytoplankton concentration levels throughout the region. The first three cycles of P1408 were conducted in waters near Point Conception. However, Chl and primary productivity levels were more representative of oligotrophic, offshore regions than normal conditions in the coastal region. Cycles 1408-4 and 1408-5 were conducted further from shore and also had low phytoplankton biomass and warm temperatures. The P1408 cruise had the lowest Aulosphaeridae abundances in our dataset. Cycles 1408-1, 1408-2, and 1408-3 all had peak concentrations in the 7–13 cells m^{-3} range; 1408-4 and 1408-5 had concentrations < 1 cell m^{-3}.

The P1604 cruise was conducted at the end of the 2015–2016 El Niño as temperature and upwelling conditions were starting to return to normal, but plankton community composition was still influenced by the El Niño. Cycles 1604-1 and 1604-2 were conducted in offshore, oligotrophic regions. 1604-3 featured intermediate productivity and biomass. 1604-4 occurred very near Point Conception and had very high surface nutrient, Chl, and mesozooplankton biomass. Aulosphaeridae abundance was lower on 1604-2 (max of ~ 20 cells m^{-3}) than the other cycles (max of ~ 40 cells m^{-3}). 1604-3 was notable for having the shallowest peak Aulosphaeridae concentration (~ 50 m, which was still beneath the euphotic zone) in our entire dataset. Typically Aulosphaeridae peak abundances were at ~ 100–120 m (Fig. 3).

Aulosphaeridae were typically found in water that was ~ 10°C (Fig. 4a). However, on P1106 the peak abundance was at ~ 9°C and on the P1604 Cruise there was a bimodal peak with organisms on Cycle 1604-3 having maximum abundances at ~ 11°C and the other cycles typically at 9°C (Fig. 4b). We found a negative correlation between the depth of the 10°C isotherm and Aulosphaeridae abundance (Fig. 4c). This relationship held when pooling cycles from all cruises together and when analyzing the cycles from each cruise individually, with the exception of cruise P1604. The mean ESD of Aulosphaeridae cells measured by UVP5 was 1.94 mm with a median of 1.80 mm and a standard deviation of 0.67 mm.

Aulosphaeridae growth, loss, and CD

If we assume that cell sinking is the primary loss term for Aulosphaeridae, we can calculate Aulosphaeridae turnover times (τ) by dividing vertically integrated standing stock by flux. Using 0–100 m standing stock and flux into 100-m sediment traps, we calculate that τ_{0-100} ranged from 0.04 d to 6.8 d, although the two cycles with τ_{0-100} < 1 d were both from water with very low Aulosphaeridae abundance and hence high uncertainty in turnover times (Table 1). We thus suggest that a more realistic range for turnover time is 2.1–6.8 d and exclude the two outliers from further analyses. The median of τ_{0-100} was 4.7 d, while the geometric mean was 4.2 d. For cruises P1408 and P1604, we also calculated turnover times from 150 m standing stocks and fluxes (τ_{0-150}) and found a median of 12.1 d and a geometric mean of 10.9 d. It thus seems likely that turnover time was longer (and hence growth rate was lower) for organisms living deeper in the water column. These population turnover times equate to growth rates in the range of 0.05–0.5 d^{-1}. However, growth rates calculated from τ should be considered conservative, since other processes (e.g., predation) could also lead to loss of Aulosphaeridae from the water column.

The CD of an individual Aulosphaeridae cell can be calculated from Eq. 1 using these estimates for τ. If we assume C : V of 1.1 μg C mm^{-3}, τ = 10 d and ESD = 2 mm, this suggests the CD for a 2-mm cell should be 1.2 μg C $cell^{-1}$ d^{-1}. Based on the variability in τ that we measured, CD for 2-mm cells in the 0–100 m depth range ranged from 0.8 μg C $cell^{-1}$ d^{-1} to 2.8 μg C $cell^{-1}$ d^{-1} assuming a C : V of 1.1 μg C mm^{-3} (Table 2). For cells in the 0–150 m depth range, CD ranged from 0.1–1.2 μg C $cell^{-1}$ d^{-1}. Given these estimates for CD (with a

Table 1. Aulosphaeridae abundance determined by UVP5 (average of multiple vertical casts per cycle). Cycle average Aulosphaeridae flux determined by sediment traps. Turnover time (τ). All measurements are mean ± standard error.

	Aulosphaeridae abundance (cells m^{-3})							Aulosphaeridae flux (cells m^{-2} d^{-1})		τ (d)	
Cycle	0–50 m	50–100 m	100–150 m	150–200 m	200–300 m	300–400 m	400–500 m	100 m	150 m	0–100 m	0–150 m
2008.1	30.9±6	291.5±55.8	805.1±537.9	116.6±25.7	95.4±40.9	12.7±4	21.1±7.6				
2008.2	1.2±0.6	16.7±5.5	36.2±6.4	29.7±3.1	6.2±1.4	1.7±0.5	2.5±0.6				
2008.3	10.7±4	191.1±22.1	265.6±24.1	115.5±14.2	47.9±18.5	12.7±1	10±1.3				
2008.4	5±0.9	48.9±4.8	93.8±13.3	62.3±8.4	22.1±9	4.3±0.9	4.5±0.9				
2008.5	7.4±1.8	41.3±5.6	35.2±6.3	40.4±4.3	12.7±1.8	5.3±1.3	4.5±1.1				
2008.6	13.4±4.3	46±5.1	108.6±11.4	110.7±5.4	47.5±2.9	6.5±1.2	3.2±1.2				
2011.1								1216±163			
2011.2	0.4±0.4	4.9±1.8	29.8±9.3	10.2±2.7	3.2±1.1	6.1±1.6	2.3±1.3	57±31		4.7	-
2011.3	17±11.3	206.5±33	235.3±24.7	81.5±16.1	25.5±10.2	7.1±1.1	5.7±1.7	2439±207		4.6	-
2011.4	14.3±7.1	165.3±31.6	322.8±32.2	158±30	24.4±5.6	11±2.2	3.2±1	1825±258		4.9	-
2011.5	1.7±0.7	41.7±5.8	412.6±76.2	299.4±54.4	73.6±15	11.8±2.3	3.9±1	628±106		3.5	-
2011.6	2.4±1.7	144.6±14.9	326±34.3	145.9±15.1	48.2±10.3	14.8±3.7	7.9±2.4	1944±310		3.8	-
2012.1	2.9±0.8	63±10.6	93±3.7	21.8±2.7	4.1±1.4	3.5±1.4	0.8±0.4	707±95		4.7	-
2012.2	0±0	0.7±0.3	6±2.4	3.5±1.6	0.5±0.3	0.7±0.5	1.2±0.5	756±118		0.04	-
2012.3	1.1±0.5	110.3±11	68.1±9.2	17.2±3.9	3.3±0.8	0.9±0.4	2.9±1.1	1185±143		4.7	-
2012.4	0±0	0.7±0.5	0.4±0.4	0±0	0.6±0.3	0.6±0.3	2.2±1.2	13±14		2.6	-
2012.5	2.2±1	2.8±1.9	11.3±1.7	8.3±1.4	4.2±2.8	3.6±1	3.8±1.7	60±50		4.2	-
2014.1	2.6±0.6	5.4±0.7	4.1±0.6	2.5±0.9	0.8±0.4	0.4±0.2	1.6±1	65±24		6.1	-
2014.2	1.7±0.5	10±1.5	8.4±0.8	4.8±1	2.1±0.6	0.4±0.2	0.8±0.3	94±28	132±42	6.2	7.6
2014.3	0.6±0.3	6.3±1.1	5.6±1.4	1.9±0.6	0.7±0.3	0.5±0.2	1±0.3	51±34	16±16	6.8	38.5
2014.4	0±0	0±0	0±0	0±0	0±0	0±0	0±0	0±0	0±0	-	-
2014.5	0±0	0.1±0.1	0±0	0±0	0.2±0.1	0±0	0.3±0.2	23±23	0±0	0.19	-
2016.1	0±0	6.7±2.4	31±2.7	18.6±1.7	3.6±0.3	2.3±0.8	1±0.2	121±115	178±34	2.8	10.6
2016.2	0±0	3.4±0.8	11.9±1.7	6.9±0.7	2.3±0.5	0.7±0.2	0.8±0.3	82±120	161±26	2.1	4.7
2016.3	9.8±1.6	36.9±1.4	22.3±1.4	11.7±0.8	4.1±1.1	2.3±0.4	0.2±0.1	399±97	178±36	5.9	19.4
2016.4	3.3±0.9	17.8±2.8	30.9±4.1	28.7±7.2	5.4±0.9	1±0.5	0.7±0.7	413±64	231±16	2.6	11.2
Geo mean										**4.2**	**12.1**
Median										**4.7**	**10.9**

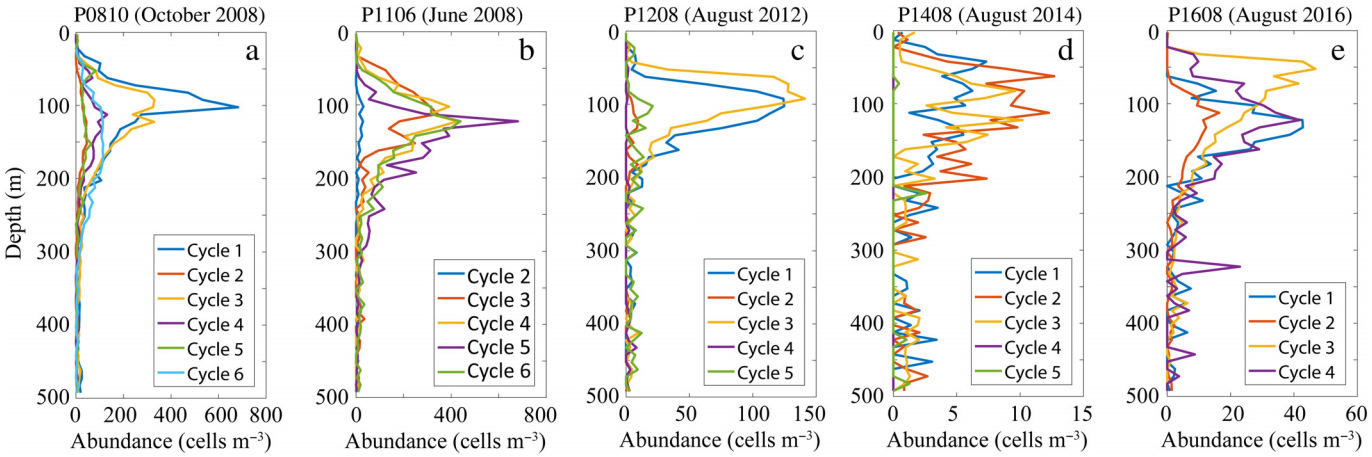

Fig. 3. Aulosphaeridae vertical profiles measured by UVP5. Each colored line is the average abundance for a Lagrangian cycle.

C : V of 1.1 μg C mm^{-3}) and the maximum cell concentrations measured on the P1106 cruise, we would expect community CD to exceed 0.5 mg C m^{-3} d^{-1} locally during Aulosphaeridae peak abundances

Aulosphaeridae carbon supply and flux remineralization

We assume that feeding by the Aulosphaeridae is primarily a passive process in which food is obtained through either random collisions with motile prey or by settling of sinking particles that are intercepted. Carbon supplied by random collisions with motile prey (diffusion feeding) can be calculated from Supporting Information Eq. A2 if we know the protistan biomass. Although protistan biomass in the twilight zone was not a consistent measurement made on our cruises, Taylor et al. (2012) measured protist biomass on a subset of stations from the P0810 cruise and found an average of 3 μg C L^{-1} at 100 m depth. We consider this a representative estimate of protistan biomass in the upper twilight zone in the CCE and hence calculate that a 2-mm Aulosphaeridae cell would be able to consume 0.12 μg C cell^{-1} d^{-1}.

We can also calculate the carbon supplied to Aulosphaeridae by sinking particles from Eq. 2 and Supporting Information Eq. A1 if we know the length: width ratios of sinking particles in the CCE. Using measurements made of the length and width of individual fecal pellets collected during sediment trap deployments in the CCE (Fig. 5), we calculated that the carbon flux-weighted mean of D_{par} (the effective interception diameter for a rotating oblate sphere, *see* Eq. A1 and the Supporting Information Appendix) was 403 μm for sinking fecal pellets. We can thus calculate that for a 2-mm Aulosphaeridae cell, the interception area for sinking particles is 6.6 mm^2. Based on measured vertical carbon flux, a typical 2-mm cell living at a depth between the base of the euphotic zone and 100 m would have intercepted 0.3–2.4 μg C cell^{-1} d^{-1}. Cells living between 100 m and 150 m would have intercepted 0.2–1.6 μg C cell^{-1} d^{-1}.

Regardless of the depth range, it is clear that Aulosphaeridae are deriving more of their nutrition from flux feeding than from diffusion feeding. Summing carbon supply from these two feeding modes allows us to estimate total supply to an Aulosphaeridae cell. Total C supply ranged from 0.3 μg C cell^{-1} d^{-1} to 2.5 μg C cell^{-1} d^{-1} (Table 2). This carbon supply was often sufficient to meet the CD of an Aulosphaeridae cell if we assume a C : V ratio of 1.1 μg C mm^{-3} (the median value of carbon supply: demand was 0.80, Fig. 6).

The cross-sectional area over which an individual Aulosphaeridae cell collects sinking particles can be computed for each cell measured in the UVP5. As noted above, for a 2-mm cell the collection area is 6.6 mm^2 (Supporting Information Eq. A1). Because we have high resolution profiles of Aulosphaeridae abundance (with morphometric data, including ESD, for each cell), we can compute the fraction of sinking particles that would be intercepted by the Aulosphaeridae community as a function of depth using Eq. 3. Due to the high inter-cruise variability in Aulosphaeridae abundance, their impact on particle flux attenuation was highly variable; on P1408 they intercepted < 1% of sinking particles, on 1106-4 and 1106-6 Aulosphaeridae would have intercepted > 20% of sinking particles produced in the euphotic zone before those particles reached a depth of 300 m (Fig. 7). From these estimates of cumulative percentage of flux intercepted, we can also calculate an effective remineralization length constant for sinking particles with respect to their collection by Aulosphaeridae (λ_{Aul}). λ_{Aul} was highly variable, reaching a peak value (for the depth range of 50–150 m), of 1.8×10^{-3} m^{-1} (Table 2). At its highest values, λ_{Aul} exceeded the remineralization length constant for sinking organic carbon determined directly from sediment traps (λ_{tot}), although we note that not all organic carbon consumed by Aulosphaeridae will be respired to CO_2. The ratio of λ_{Aul} : λ_{tot} gives an estimate of the proportional role of Aulosphaeridae in twilight zone flux attenuation. The geometric mean of this ratio was substantial for the P0810 and P1106 cruises

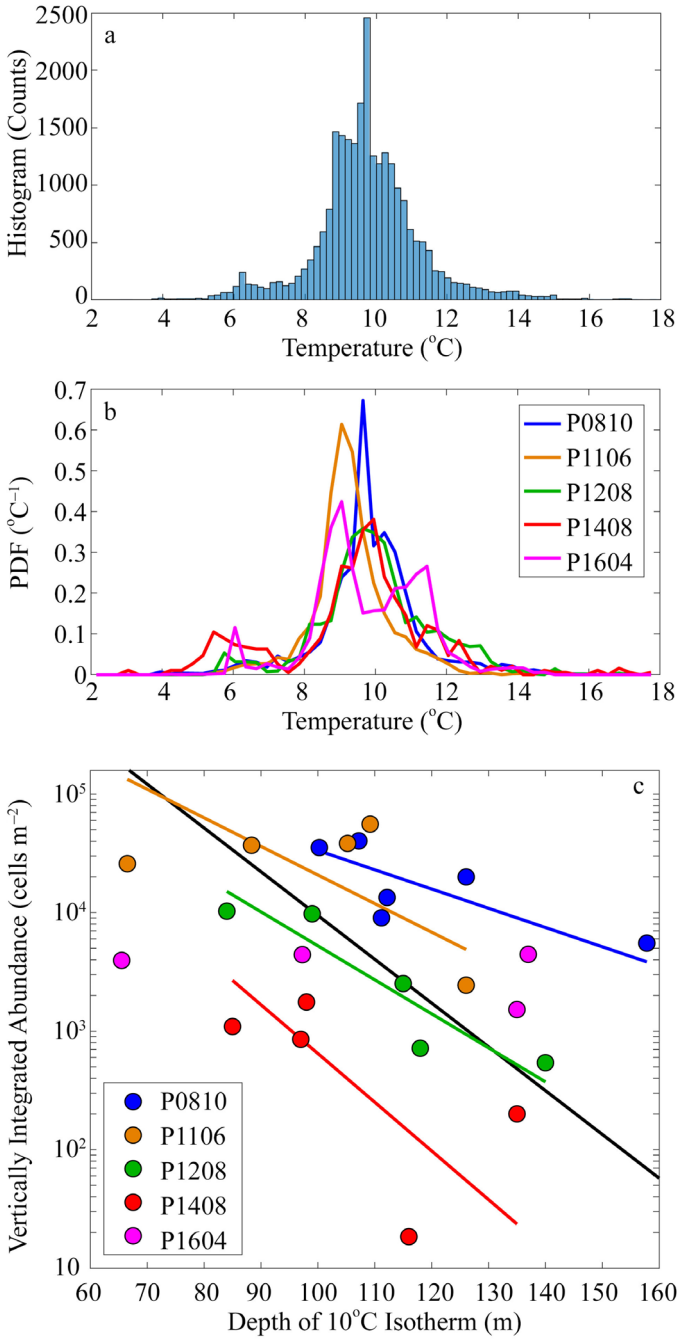

Fig. 4. Histogram of temperatures for each Aulosphaeridae encountered (**a**). Probability density function for temperatures of Aulosphaeridae for each individual cruise (**b**). Aulosphaeridae abundance plotted against the depth of the 10°C isotherm (**c**). Black regression line is a Type II geometric mean regression of $\log_{10}$(abundance) against depth. Correlation coefficient is –0.31. Colored lines are regressions for individual years. Correlation coefficients are –0.75 (2008), –0.52 (2011), –0.93 (2012), and –0.65 (2014).

(0.26 and 0.10, respectively) and low for the other cruises (0.024, 0.001, and 0.019 for P1208, P1408, and P1604, respectively).

Discussion

The ecological role of Aulosphaeridae

Equations 2 and 4, combined with estimates of protistan biomass and vertical carbon flux in the CCE suggest that Aulosphaeridae nutrition is predominantly derived from sinking particles. However, if a carbon density of 80 μg C mm^{-3} is assumed (as used in previous global estimates of rhizarian biomass), Aulosphaeridae cells cannot obtain enough nutrition to satisfy their CD as defined by Eq. 1 (Fig. 6). The carbon : volume ratio of the Aulosphaeridae cells should be considered highly uncertain at this time. Accurate measurement of rhizarian carbon biomass requires meticulous collection techniques (typically by in situ divers) to ensure that individuals are retrieved intact (Michaels et al. 1995). These methods require major investments of ship time and personnel and are not feasible for taxa that are not abundant in the surface layer. Such measurements have shown widely varying carbon : volume ratios for rhizarians (including acantharians, foraminiferans, and polycystine radiolarians) from the Sargasso Sea (Michaels et al. 1995). Based on the carbon supply : CD ratio calculated in Table 2 and Fig. 6, we suggest that the C : V ratio determined by assuming most of the cellular carbon is in the central capsule (1.1 μg C mm^{-3}) is a reasonable estimate, because with this value the carbon supply and demand of Aulosphaeridae would be nearly balanced. This C : V value is nearly two orders of magnitude lower than the estimate of 80 μg C mm^{-3} used by Biard et al. (2016) in their global estimate of rhizarian biomass. However, it is similar to measurements of acantharian C : V and the estimated C : V ratio for the central capsule itself (~ 60 μg C mm^{-3}; Menden-Deuer and Lessard 2000) is within the range of central capsule-based C : Vs measured for solitary polycystine radiolarians (9–280 μg C mm^{-3}; Michaels et al. 1995). It thus seems likely that most of the carbon contained in Aulosphaeridae is within the central capsule (which comprises only ~ 1.6% of the scleracoma that is typically used to estimate cellular biovolume) leading to a much lower C : V ratio (~ 1 μg C mm^{-3}) than would be expected for a smaller protist or a crustacean zooplankton. Next, we consider possible alternate hypotheses that could enable an Aulosphaeridae cell to reach its CD with a higher C : V ratio.

From Eq. 2 and Supporting Information Eq. A2, it is clear that several additional variables impact the balance between carbon supply and demand: GGE, τ, and ESD_{eff}. Increased GGE would decrease the CD of a cell. However, we already use an above average estimate for GGE (40%), thus we consider it unlikely that an underestimate of GGE is leading to the discrepancy. Another possibility is that we are underestimating τ and hence overestimating Aulosphaeridae growth rates. Again this seems unlikely, because sinking is not the only potential mortality term for Aulosphaeridae. Aulosphaeridae have been observed in the guts of some mesozooplankton (Gowing 1989; Gowing and Coale 1989) and the rapid dissolution of their tests presents the possibility that some may dissolve

Table 2. Sediment trap organic carbon flux, remineralization length constant determined from sediment trap data (λ_{tot}), CD of a 2-mm Aulosphaeridae cell (assuming a C : V ratio of 1.1 μg C mm^{-3}), carbon supply to a 2-mm Aulosphaeridae cell (CS_{FF} + CS_{RW}, Eq. 2 and Supporting Information Eq. A2), Aulosphaeridae remineralization length constant determined from percentage of sinking particles intercepted by Aulosphaeridae in the 50–150 m depth range (λ_{Aul}). For shallow sediment traps: a = 50 m, b = 60 m, c = 70 m depth, *negative value excluded from geometric mean calculation.

	Sediment trap organic carbon flux (mg C m^{-2} d^{-1})				Aulosphaeridae CD (μg C cell^{-1} d^{-1})		Aulosphaeridae carbon supply (μg C cell^{-1} d^{-1})		
Cycle	Shallow	100 m	150 m	λ_{tot} (m^{-1})	0–100 m	0–150 m	< 100 m	100–150 m	λ_{Aul} (m^{-1})
2008.1	112±20[a]	74±6	-	8.3×10^{-3}	-	-	0.7	0.5	1.89×10^{-3}
2008.2	-	69±7	-	-	-	-	0.6	0.5	0.17×10^{-3}
2008.3	120±7[b]	78±4	-	10.7×10^{-3}	-	-	0.8	0.5	1.36×10^{-3}
2008.4	216±3[a]	149±21	-	7.5×10^{-3}	-	-	1.3	0.9	0.43×10^{-3}
2008.5	128±16[b]	127±13	-	0.1×10^{-3}	-	-	1	1	0.25×10^{-3}
2008.6	112±7[b]	107±3	-	1.2×10^{-3}	-	-	0.8	0.8	0.45×10^{-3}
2011.1	218±24[b]	184±27	-	4.2×10^{-3}	-	-	1.4	1.2	-
2011.2	-	70±5	-	-	1.2	-	0.6	0.5	0.07×10^{-3}
2011.3	409±25[b]	89±14	-	38.2×10^{-3}	1.3	-	1.5	0.4	1.07×10^{-3}
2011.4	201±29[a]	61±17	-	23.8×10^{-3}	1.2	-	0.9	0.4	1.74×10^{-3}
2011.5	-	101±9	-	-	1.7	-	0.8	0.7	0.71×10^{-3}
2011.6	282[b]	248±49	-	3.2×10^{-3}	1.5	-	1.9	1.6	1.62×10^{-3}
2012.1	437±14[b]	299±18	-	9.5×10^{-3}	1.2	-	2.5	1.7	0.86×10^{-3}
2012.2	150±39[c]	121±5	-	7.1×10^{-3}	-	-	1	0.8	0.03×10^{-3}
2012.3	150±19[b]	111±21	-	7.5×10^{-3}	1.2	-	1	0.7	0.97×10^{-3}
2012.4	-	133±11	-	-	2.2	-	1	0.9	0.01×10^{-3}
2012.5	328[c]	152±27	-	25.6×10^{-3}	1.4	-	1.6	0.7	0.16×10^{-3}
2014.1	158±8[b]	159±16	-	-0.1×10^{-3}*	0.9	-	1.2	1.2	0.04×10^{-3}
2014.2	124±14[b]	80±13	64±3	7.4×10^{-3}	0.9	0.8	0.8	0.6	0.07×10^{-3}
2014.3	111±11[b]	43±3	48±9	12.8×10^{-3}	0.8	0.1	0.7	0.4	0.04×10^{-3}
2014.4	51±2[c]	39±5	29±6	7.4×10^{-3}	-	-	0.4	0.3	0×10^{-3}
2014.5	-	42±1	27±1	9.2×10^{-3}	-	-	0.6	0.3	0×10^{-3}
2016.1	-	72±7	32±5	16.4×10^{-3}	2.1	0.5	1.3	0.4	0.11×10^{-3}
2016.2	-	40±4	37±5	1.6×10^{-3}	2.8	1.2	0.4	0.4	0.04×10^{-3}
2016.3	120±10[b]	91±2	77±4	4.8×10^{-3}	1.0	0.3	0.8	0.7	0.13×10^{-3}
2016.4	251±8[a]	255±55	202±14	2.9×10^{-3}	2.3	0.5	1.8	1.6	0.11×10^{-3}
Geo mean				6.2×10^{-3}	1.5	0.6	1.1	0.8	0.17×10^{-3}
Median				7.5×10^{-3}	1.2	0.5	0.9	0.7	0.16×10^{-3}

before reaching our trap depths. Our median computed turnover times (4.7 d at 100 m; 10.9 d at 150 m) are also consistent with average turnover times estimated for radiolarian standing stocks from 30°S to 30°N (10–15 d; Boltovskoy 2017) and for rhizarians in the Sargasso Sea (6 d for Foraminifera; 40 d for Acantharia; Michaels et al. 1995). It is also possible that our sediment traps underestimate sinking flux. However, the good agreement between ^{234}Th flux calculated from ^{238}U-^{234}Th disequilibrium and ^{234}Th flux measured in the sediment traps suggests that the traps have no substantial bias and that any particles missed by the trap would have to contain negligible ^{234}Th (Stukel et al. 2013, 2015). Furthermore, vertical flux sufficient to meet Aulosphaeridae demand (assuming a C : V ratio of 80 μg C mm^{-3}) would require sinking carbon flux in excess of euphotic zone vertically integrated primary productivity rates. A more plausible possibility is that we are under-estimating ESD_{eff}. ESD_{eff} depends on two independent factors: the cross-sectional collection area of the Aulosphaeridae and the size of sinking particles (or aggregates) that it is collecting. We have assumed that the collection area of Aulosphaeridae is equivalent to the area of a circle defined by the maximum extent of its siliceous spicules (thus assuming that it is larger than the diameter used for biovolume). However, some solitary polycystine radiolarians produce pseudopodial extensions that allow them to increase their effective collection area (Anderson and Botfield 1983; Anderson et al. 1986). Increasing its collection area sufficiently to meet its carbon supply (at a C : V ratio of 80 μg C mm^{-3}) would require a ~ ×80 increase in area or ~ ×9 increase in ESD. While extensive pseudopodial networks have been observed in some

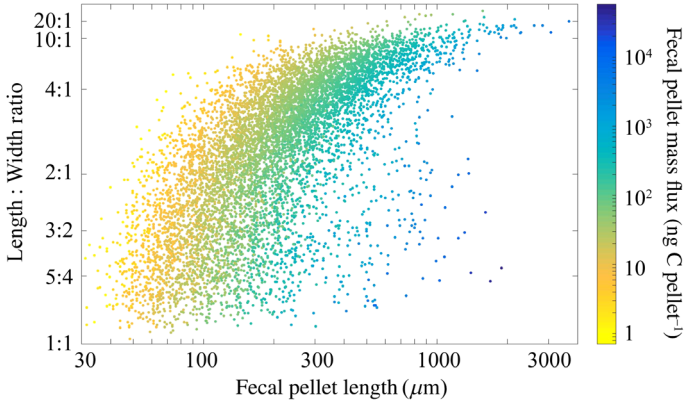

Fig. 5. Length : width ratios of fecal pellets collected in sediment traps.

Rhizaria (Anderson et al. 1986), they have not been observed for Phaeodaria (Anderson et al. 1986; Nakamura and Suzuki 2015). Furthermore, the results from the phaeodarian peak encountered on our P1106 cruise offer powerful constraints for testing this hypothesis. On Cycles 1106-4 and 1106-6, we calculated that Aulosphaeridae could intercept > 15% of sinking particles produced in the euphotic zone before they reach a depth of 150 m. If the collection area of individual cells were ×80 higher than we had calculated, Aulosphaeridae would intercept > 99.99% of sinking particles before they reached a depth of 150 m on these two cycles (and > 99% of flux on six other cycles). This is clearly unrealistic, given measured carbon flux attenuation in the region (Table 2). Furthermore, if a C : V of 80 μg C mm^{-3} ratio is accurate, the CD of the entire Aulosphaeridae community would exceed 750 mg C m^{-2} d^{-1} for two cycles on P1106 even if we assumed that the lower turnover times calculated from the 150 m traps were representative of the community. These values are clearly unrealistic as export at 100 m depth averaged 113 mg C m^{-2} d^{-1} on P1106 and total primary productivity was less than 1000 mg C m^{-2} d^{-1}.

Based on our revised C : V ratio (1.1 μg C mm^{-3}), we can make a revised estimate of the biomass of Aulosphaeridae (the dominant large rhizarian in the CCE). Across the 25 Lagrangian experiments for which we have UVP5 profiles, the biomass of Aulosphaeridae in the upper 500 m of the water column ranged from 0 mg C m^{-2} to 52 mg C m^{-2} with a median of 4.5 mg C m^{-2} and an arithmetic mean of 13 mg C m^{-2}. For comparison, mesozooplankton biomass determined from oblique bongo net tows to a depth of 210 m during our Lagrangian experiments typically ranged from 500 mg C m^{-2} to 2000 mg C m^{-2}. It is thus clear that the relative contribution of Aulosphaeridae to total mesozooplankton biomass in the CCE ranges from 0% to ~ 10%, although their relative contribution to mesozooplankton biovolume and abundance is much greater.

Our estimate of low C : V ratios for Aulosphaeridae also has implications for the ecological role of these abundant taxa.

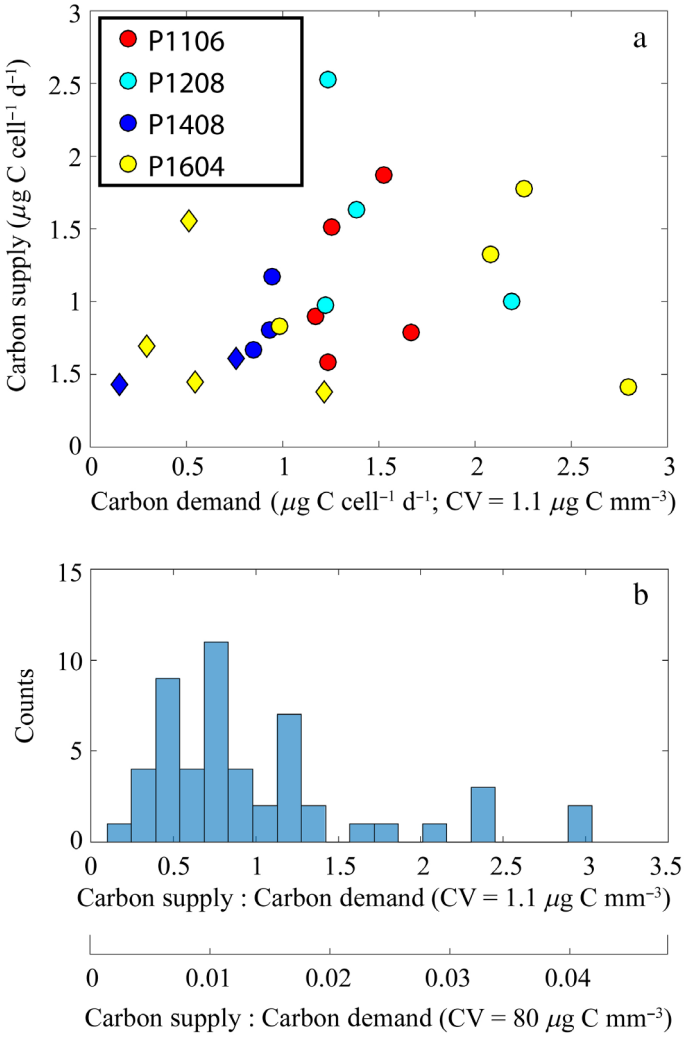

Fig. 6. (**a**) CD and carbon supply to a 2-mm Aulosphaeridae cell assuming a carbon : volume ratio of 1.1 μg C mm^{-3}. Circles are calculated for < 100 m cells; diamonds are for < 150 m cells. (**b**) Histogram of the ratio of carbon supply: demand assuming a carbon : volume ratio of either 1.1 μg C mm^{-3} (upper *x*-axis) or 80 μg C mm^{-3} (lower *x*-axis). For cycle/depth combinations for which sediment trap data were not available for estimating τ, we assumed the median τ for the appropriate depth (4.7 d for 100 m; 10.9 d for 150 m).

Our results suggest that Aulosphaeridae have moderate growth rates that decline with depth. This decline with depth is likely caused by both a decrease in temperature with depth (temperature typically declined from 12–16°C at 50 m, to 9–11°C at 100 m and 8.5–9°C at 150 m) and a decrease in food supply with depth. These organisms derive most of their nutrition from the rain of sinking particles from above. Normally, such a feeding strategy would not be advantageous for a large organism, since food supply (in the food-limited twilight zone) is related to the cross-sectional area and food demand is related to the volume of the organism. However, Aulosphaeridae seem to use their large scleracoma to support a low carbon-density ectoplasm that effectively increases their

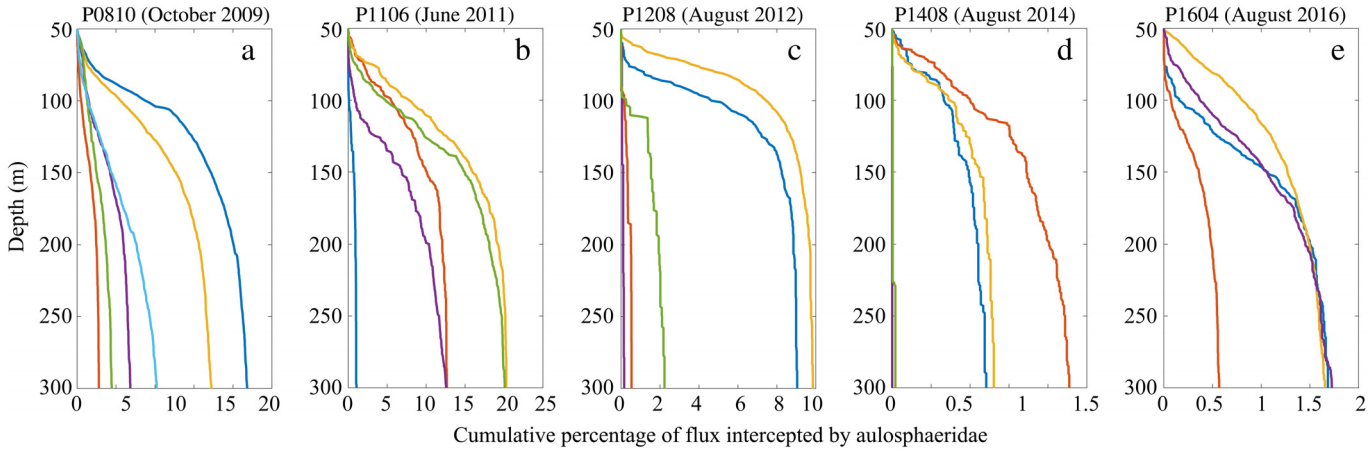

Fig. 7. Aulosphaeridae flux attenuation calculated from Eq. 3. X-axis is the cumulative percentage of particles produced in the surface 50 m that would be intercepted by Aulosphaeridae cells. Line colors among cruises are as in Fig. 3.

collection area without substantially increasing their biomass, which is primarily contained within their central capsule.

The low carbon and biogenic silica density of Aulosphaeridae is also an elegant evolutionary adaptation to the problem of maintaining buoyancy for a large cell. Following Baines et al. (2010), the excess density of a cell can be calculated from the excess density of biogenic silica (2.15 g mL^{-1}) and organic matter (1.05 g mL^{-1}) and the relative proportion of the cellular volume comprised by cytoplasm and the siliceous test. Based on our estimate of the carbon content of Aulosphaeridae (1.1 μg C mm^{-3}), the Si content of Aulosphaeridae quantified by Biard et al. (2018; ~ 10 μg Si $cell^{-1}$) and our estimate that the effective radius of Aulosphaeridae extends 25% beyond the volume of the central sphere of the scleracoma, we calculate that the excess density of Aulosphaeridae cells is 0.72 μg mm^{-3}. However, if we assumed that Aulosphaeridae had a similar Si : volume ratio to typical diatoms (20 μg Si mm^{-3}; Conley et al. 1989) and the carbon density assumed by Biard et al. (2016), Aulosphaeridae excess density would be 11.7 μg mm^{-3}, which would imply a sinking rate ×16 higher than we calculate based on our Si and carbon values. Even if the Si content measured by Biard et al. (2018) were combined with a carbon density of 80 μg C mm^{-3}, we would calculate an excess density of 6.9 μg mm^{-3} that implies a sinking rate ×9.6 higher than we calculate based on our carbon : volume estimate. The low carbon and biogenic silica-density thus effectively decrease population loss due to sinking or, alternatively, the amount of energy that must be utilized to maintain their buoyancy. Additionally, this low-density silica strategy would lead to a lower preservation efficiency than more heavily silicified plankton (e.g., diatoms, polycystine radiolarians), which use their shell for protection and buoyancy regulation (Raven and Waite 2004). This insight helps to explain why many Phaeodaria are not preserved in the sediment record and why their contribution to biogenic silica export has not been considered important until recently (Biard et al. 2018).

Other Phaeodarian taxa have been shown to have strong temperature associations (Meyer 1933; Nakamura et al. 2013; Nakamura and Suzuki 2015) and this is likely true for the Aulosphaeridae taxa in our study. We find that their abundance is greatest in water temperatures between 9°C and 11°C and that their spatial variability within a cruise is inversely correlated with the depth of the 10°C isotherm. This temperature-dependence likely leads to the large temporal variability in the dataset as well; the P1408 cruise, with the warmest region-wide temperatures had the lowest Aulosphaeridae abundance, while the two coolest cruises (P0810 and P1106) had the highest Aulosphaeridae abundance. It is perhaps surprising that we see such stark declines in Aulosphaeridae abundance as the 10°C isotherm deepens, instead of simply a deepening of the depth of residence of these organisms. We surmise that decreased food availability or oxygen levels or some unknown physical or chemical conditions may prevent optimal growth at deeper depths. Nevertheless, it seems that the prevalence of anomalously warm periods in our study (P1408 and P1604) may lead to an underestimate of regional average Aulosphaeridae abundance relative to the climatological mean.

Twilight zone CD and flux attenuation

The mesopelagic zone contains a wide diversity of organisms evolved to exist in a food-poor environment. This ecosystem is largely dependent on energy derived from the euphotic zone and transported to depth within sinking particles or through the vertical migrations of metazoan taxa (Steinberg et al. 2008*b*; Robinson et al. 2010). However, major questions surrounding mesopelagic carbon cycling remain. Specifically, most studies to date have found a substantial deficit of carbon transport to the deep ocean, relative to the demand of organisms living in this ecosystem (Burd et al. 2010). For instance, at sites in the subtropical and subarctic Pacific, both bacterial CD and mesozooplankton CD substantially exceeded the supply of sinking particles to midwater depths (Steinberg

et al. 2008*b*). Within the CCE, the recently quantified and substantial metabolism of myctophids and other midwater fishes require even greater carbon flux (Davison et al. 2013). Using the turnover times derived from our 100 m sediment traps and the conservative C : V ratio (1.1 μg C mm^{-3}), we still find a substantial CD for the Aulosphaeridae community, peaking at 27 mg C m^{-2} d^{-1} on cycle 1106-4 with a cruise-wide average of 16 mg C m^{-2} d^{-1}. These conservative estimates of Aulosphaeridae CD must be added to the already-demonstrated demand of bacteria, mesozooplankton, and mesopelagic fish and reconciled with the relatively low rates of carbon exported out of the euphotic zone on sinking particles (~ 100 mg C m^{-2} d^{-1} in the CCE, Table 2). The imbalance between supply and demand suggests that other transport mechanisms must be important. Likely processes include active transport by diel vertically migrating organisms (Steinberg et al. 2000; Davison et al. 2013; Stukel et al. 2013) and advective and diffusive transport of POM and DOM (Carlson et al. 1994; Omand et al. 2015; Stukel et al. 2018), both of which have been shown to be quantitatively important in the CCE.

The high abundances and large cross-sectional area of Aulosphaeridae also imply a substantial role in intercepting and remineralizing sinking particles (Fig. 6). Twilight zone flux attenuation can play an important role in modulating the impact of the biological pump (Martin et al. 1987; Buesseler and Boyd 2009). Globally a 24-m increase in the depth at which 63% of sinking organic carbon has been remineralized can lead to a 10–27 ppm decrease in atmospheric CO_2 levels (Kwon et al. 2009). We found that, while Aulosphaeridae abundance was highly variable, they can at times intercept > 20% of the particles exported from the euphotic zone and be responsible for a substantial portion of flux attenuation in the shallow mesopelagic. Their variability may thus impact the carbon remineralization length scale and hence carbon sequestration patterns in the CCE. We also note that our current study assesses the impact of only a single group of Rhizaria. Other taxa may also play substantial roles. For instance, Castanellidae is another phaeodarian family that was not included in this study because its size is on the lower limit of detection for the UVP5. However, this group was even more abundant in sediment trap samples than Aulosphaeridae and actually has greater silica content per cell (Biard et al. 2016, 2018). Similarly, genetic analyses have shown that radiolarian sequences are more abundant than phaeodarian sequences in both sediment trap material and the overlying water column in the CCE (Gutierrez-Rodriguez et al., unpubl.). Clearly, these other organisms must play a substantial role that further inflates the importance of under-studied Rhizaria to global carbon and nutrient cycles.

Conclusions

Our integrated quasi-Lagrangian sampling scheme, coupled with the use of modern in situ imaging technology, allows us an unprecedented ability to quantify the ecological and biogeochemical role of fragile phaeodarians in the twilight zone. Across a range of conditions varying from coastal to oligotrophic, spring to fall, and El Niño to ENSO-neutral, we find that Aulosphaeridae abundances are highly variable in time and that this variability is likely driven by a preference for periods when 9–10°C water is abundant in the depths immediately below the euphotic zone. Despite these large changes in abundance, we find similar turnover times between cruises, which imply growth rates that are typically in the range of 0.05–0.5 d^{-1}. In comparison with contemporaneous carbon flux measurements, we find that carbon supply to Aulosphaeridae can only meet these organisms' CD if a low C : V ratio is used (~ 1 μg C mm^{-3}). This C : V ratio is sensible if we assume that most of the carbon is contained within the central capsule of the cell, while the large siliceous test serves to substantially increase the cross-sectional area of the cell without concomitant increase in cellular carbon biomass. This reduced C : V ratio suggests that, if true for other taxa, the global biomass of large Rhizaria needs to be revised downwards. New determinations of the C : V relationship across a range of cell sizes of phaeodarians, polycystine radiolarians, and other Rhizaria are urgently needed. However, our results also show that, despite this decreased biomass, Aulosphaeridae play a substantial role in twilight zone flux attenuation and at maximum concentrations they can intercept > 20% of sinking particles produced in the euphotic zone before these particles reach a depth of 300 m. Since Aulosphaeridae are only one of many different rhizarian taxa that live in the CCE, it is clear that the Rhizaria deserve greater attention and a concerted effort to elucidate their variability and role in the biological pump.

References

Anderson, O. R., and M. Botfield. 1983. Biochemical and fine structure evidence for cellular specialization in a large spumellarian radiolarian *Thalassicolla nucleata*. Mar. Biol. **72**: 235–241. doi:10.1007/BF00396828

Anderson, O. R., N. R. Swanberg, J. Lindsey, and P. Bennett. 1986. Functional morphology and species characteristics of a large, solitary radiolarian *Physematium muelleri*. Biol. Bull. **171**: 175–187. doi:10.2307/1541915

Baines, S. B., B. S. Twining, M. A. Brzezinski, D. M. Nelson, and N. S. Fisher. 2010. Causes and biogeochemical implications of regional differences in silicification of marine diatoms. Global Biogeochem. Cycles **24**: GB4031. doi: 10.1029/2010gb003856

Beers, J. R., and G. L. Stewart. 1970. The ecology of the plankton off La Jolla, California, in the period April through September, 1967. Bull. Scripps Inst. Oceanogr. **17**: 67–87.

Biard, T., and others. 2016. In situ imaging reveals the biomass of giant protists in the global ocean. Nature **532**: 504–507. doi:10.1038/nature17652

Biard, T., J. W. Krause, M. R. Stukel, and M. D. Ohman. 2018. The significance of giant Phaeodarians (Rhizaria) to biogenic silica export in the California Current Ecosystem. Global Biogeochem. Cycles. **32**. doi:10.1029/2018GB005877

Boltovskoy, D. 2017. Vertical distribution patterns of Radiolaria Polycystina (Protista) in the World Ocean: Living ranges, isothermal submersion and settling shells. J. Plankton Res. **39**: 330–349. doi:10.1093/plankt/fbx003

Boltovskoy, D., S. A. Kling, K. Takahashi, and K. Bjorklund. 2010. World atlas of distribution of recen polycystina (radiolaria). Palaeontologia Electronica, 13.

Boyd, P. W., and T. W. Trull. 2007. Understanding the export of biogenic particles in oceanic waters: Is there consensus? Prog. Oceanogr. **72**: 276–312. doi:10.1016/j.pocean.2006.10.007

Buesseler, K. O., and others. 2007. Revisiting carbon flux through the ocean's twilight zone. Science **316**: 567–570. doi:10.1126/science.1137959

Buesseler, K. O., and P. W. Boyd. 2009. Shedding light on processes that control particle export and flux attenuation in the twilight zone of the open ocean. Limnol. Oceanogr. **54**: 1210–1232. doi:10.4319/lo.2009.54.4.1210

Burd, A. B., and others. 2010. Assessing the apparent imbalance between geochemical and biochemical indicators of meso- and bathypelagic biological activity: What the @$#! Is wrong with present calculations of carbon budgets? Deep-Sea Res. II **57**: 1557–1571. doi:10.1016/j.dsr2.2010.02.022

Carlson, C. A., H. W. Ducklow, and A. F. Michaels. 1994. Annual flux of dissolved organic carbon from the euphotic zone in the northwestern Sargasso Sea. Nature **371**: 405–408. doi:10.1038/371405a0

Caron, D. A., P. D. Countway, A. C. Jones, D. Y. Kim, and A. Schnetzer. 2012. Marine protistan diversity, p. 467–493. *In* C. A. Carlson and S. J. Giovannoni [eds.], Annual review of marine science, v. 4. Annual Reviews.

Conley, D. J., S. S. Kilham, and E. Theriot. 1989. Differences in silica content between marine and freshwater diatoms. Limnol. Oceanogr. **34**: 205–212. doi:10.4319/lo.1989.34.1.0205

Crawford, D. W. 1992. Metabolic cost of motility in planktonic protists: Theoretical considerations on size scaling and swimming speed. Microb. Ecol. **24**: 1–10. doi:10.1007/BF00171966

Davison, P. C., D. M. Checkley, J. A. Koslow, and J. Barlow. 2013. Carbon export mediated by mesopelagic fishes in the Northeast Pacific Ocean. Prog. Oceanogr. **116**: 14–30. doi:10.1016/j.pocean.2013.05.013

Ducklow, H. W., D. K. Steinberg, and K. O. Buesseler. 2001. Upper Ocean carbon export and the biological pump. Oceanography **14**: 50–58. doi:10.5670/oceanog.2001.06

Gorsky, G., and others. 2010. Digital zooplankton image analysis using the ZooScan integrated system. J. Plankton Res. **32**: 285–303. doi:10.1093/plankt/fbp124

Gowing, M. M. 1986. Trophic biology of phaeodarian radiolarians and flux of living radiolarians in the upper 2000 m of the North Pacific central gyre. Deep-Sea Res. **33**: 655–674. doi:10.1016/0198-0149(86)90059-2

Gowing, M. M. 1989. Abundance and feeding ecology of Antarctic phaeodarian radiolarians. Mar. Biol. **103**: 107–118. doi:10.1007/BF00391069

Gowing, M. M., and S. L. Coale. 1989. Fluxes of living radiolarians and their skeletons along a Northeast Pacific transect from coastal upwelling to open ocean waters. Deep-Sea Res. **36**: 561–576. doi:10.1016/0198-0149(89)90006-X

Gowing, M. M., and K. Wishner. 1992. Feeding ecology of benthopelagic zooplankton on an eastern tropical Pacific seamount. Mar. Biol. **112**: 451–467. doi:10.1007/BF00356291

Gowing, M. M., and W. N. Bentham. 1994. Feeding ecology of phaeodarian radiolarians at the VERTEX North Pacific time series site. J. Plankton Res. **16**: 707–719. doi:10.1093/plankt/16.6.707

Harvey, E. L., H. J. Jeong, and S. Menden-Deuer. 2013. Avoidance and attraction: Chemical cues influence predator-prey interactions of planktonic protists. Limnol. Oceanogr. **58**: 1176–1184. doi:10.4319/lo.2013.58.4.1176

Honjo, S., S. J. Manganini, R. A. Krishfield, and R. Francois. 2008. Particulate organic carbon fluxes to the ocean interior and factors controlling the biological pump: A synthesis of global sediment trap programs since 1983. Prog. Oceanogr. **76**: 217–285. doi:10.1016/j.pocean.2007.11.003

Ikenoue, T., K. R. Bjorklund, S. B. Kruglikova, J. Onodera, K. Kimoto, and N. Harada. 2015. Flux variations and vertical distributions of siliceous Rhizaria (Radiolaria and Phaeodaria) in the western Arctic Ocean: Indices of environmental changes. Biogeosciences **12**: 2019–2046. doi:10.5194/bg-12-2019-2015

Kiorboe, T. 2008. A mechanistic approach to plankton ecology. Princeton Univ. Press.

Kiorboe, T., H. P. Grossart, H. Ploug, and K. Tang. 2002. Mechanisms and rates of bacterial colonization of sinking aggregates. Appl. Environ. Microbiol. **68**: 3996–4006. doi:10.1128/aem.68.8.3996-4006.2002

Knauer, G. A., J. H. Martin, and K. W. Bruland. 1979. Fluxes of particulate carbon, nitrogen, and phosphorus in the upper water column of the Northeast Pacific. Deep-Sea Res. **26**: 97–108. doi:10.1016/0198-0149(79)90089-X

Krause, J. W., M. A. Brzezinski, R. Goericke, M. R. Landry, M. D. Ohman, M. R. Stukel, and A. G. Taylor. 2015. Variability in diatom contributions to biomass, organic matter production and export across a frontal gradient in the California Current Ecosystem. J. Geophys. Res. Oceans **120**: 1032–1047. doi:10.1002/2014jc010472

Kwon, E. Y., F. Primeau, and J. L. Sarmiento. 2009. The impact of remineralization depth on the air-sea carbon balance. Nat. Geosci. **2**: 630–635. doi:10.1038/NGEO612

Lampitt, R., I. Salter, and D. Johns. 2009. Radiolaria: Major exporters of organic carbon to the deep ocean. Global Biogeochem. Cycles **23**: 1–9. doi:10.1029/2008GB003221

Landry, M. R., M. D. Ohman, R. Goericke, M. R. Stukel, and K. Tsyrklevich. 2009. Lagrangian studies of phytoplankton growth and grazing relationships in a coastal upwelling ecosystem off Southern California. Prog. Oceanogr. **83**: 208–216. doi:10.1016/j.pocean.2009.07.026

Landry, M. R., M. D. Ohman, R. Goericke, M. R. Stukel, K. A. Barbeau, R. Bundy, and M. Kahru. 2012. Pelagic community responses to a deep-water front in the CaliforniaCurrent Ecosystem: Overview of the A-Front Study. J. Plankton Res. **34**: 739–748. doi:10.1093/plankt/fbs025

Landry, M. R., and California Current Ecosystem LTER. 2017. Picophytoplankton and bacteria total carbon estimates from cell counts analyzed with flow cytometry (FCM) from CCE LTER process cruises in the California Current region, 2006–2014 (ongoing). doi:10.6073/pasta/e99666abc0a98757d78edda88f68313e

Martin, J. H., G. A. Knauer, D. M. Karl, and W. W. Broenkow. 1987. Vertex: Carbon cycling in the Northeast Pacific. Deep-Sea Res. **34**: 267–285. doi:10.1016/0198-0149(87)90086-0

Menden-Deuer, S., and E. J. Lessard. 2000. Carbon to volume relationships for dinoflagellates, diatoms, and other protist plankton. Limnol. Oceanogr. **45**: 569–579. doi:10.4319/lo.2000.45.3.0569

Meyer, L. 1933. Die geographische Verbreitung der Tripyleen Radiolarien des Sudatlantischen Ozeans, p. 122–198. Deutsche Atlantische expedition METEOR 1925-1927. Wissenschaftenliche Ergebnisse, v. 12.

Michaels, A. F., D. A. Caron, N. R. Swanberg, F. A. Howse, and C. M. Michaels. 1995. Planktonic sarcodines (Acantharia, Radiolaria, foraminifera) in surface waters near Bermuda: Abundance, biomass and vertical flux. J. Plankton Res. **17**: 131–163. doi:10.1093/plankt/17.1.131

Nakamura, Y., I. Imai, A. Yamaguchi, A. Tuji, and N. Suzuki. 2013. *Aulographis japonica* sp. nov. (Phaeodaria, Aulacanthida, Aulacanthidae), an abundant zooplankton in the deep sea of the sea of Japan. Plankton Benthos Res. **8**: 107–115. doi:10.3800/pbr.8.107

Nakamura, Y., I. Imai, A. Yamaguchi, A. Tuji, F. Not, and N. Suzuki. 2015. Molecular phylogeny of the widely distributed marine Protists, Phaeodaria (Rhizaria, Cercozoa). Protist **166**: 363–373. doi:10.1016/j.protis.2015.05.004

Nakamura, Y., and N. Suzuki. 2015. Phaeodaria: Diverse marine cercozoans of world-wide distribution, p. 223–249. *In* S. Ohtsuka, T. Suzaki, T. Horiguchi, N. Suzuki, and F. Not [eds.], Marine protists. Springer.

Nickels, C. F., and M. D. Ohman. 2018. CCEIII: Persistent functional relationships between copepod egg production rates and food concentration through anomalously warm conditions in the California Current Ecosystem. Deep-Sea Res. I. doi: 10.1016/j.dsr.2018.07.001.

Nöthig, E.-M., and M. Gowing. 1991. Late winter abundance and distribution of phaeodarian radiolarians, other large protozooplankton and copepod nauplii in the Weddell Sea, Antarctica. Mar. Biol. **111**: 473–484. doi:10.1007/BF01319421

Ohman, M. D., J. R. Powell, M. Picheral, and D. W. Jensen. 2012. Mesozooplankton and particulate matter responses to a deep-water frontal system in the southern California current system. J. Plankton Res. **34**: 815–827. doi:10.1093/plankt/fbs028

Omand, M. M., E. A. D'Asaro, C. M. Lee, M. J. Perry, N. Briggs, I. Cetinić, and A. Mahadevan. 2015. Eddy-driven subduction exports particulate organic carbon from the spring bloom. Science **348**: 222–225. doi:10.1126/science.1260062

Picheral, M., L. Guidi, L. Stemmann, D. M. Karl, G. Iddaoud, and G. Gorsky. 2010. The underwater vision profiler 5: An advanced instrument for high spatial resolution studies of particle size spectra and zooplankton. Limnol. Oceanogr.: Methods **8**: 462–473. doi:10.4319/lom.2010.8.462

Polet, S., C. Berney, J. Fahrni, and J. A. N. Pawlowski. 2004. Small-subunit ribosomal RNA gene sequences of Phaeodarea challenge the monophyly of Haeckel's Radiolaria. Protist **155**: 53–63. doi:10.1078/1434461000164

Raven, J., and A. Waite. 2004. The evolution of silicification in diatoms: Inescapable sinking and sinking as escape? New Phytol. **162**: 45–61. doi:10.1111/j.1469-8137.2004.01022.x

Robinson, C., and others. 2010. Mesopelagic zone ecology and biogeochemistry—a synthesis. Deep-Sea Res. II **57**: 1504–1518. doi:10.1016/j.dsr2.2010.02.018

Samo, T. J., and others. 2012. Microbial distribution and activity across a water mass frontal zone in the California Current Ecosystem. J. Plankton Res. **34**: 802–814. doi:10.1093/plankt/fbs048

Silver, M. W., and M. M. Gowing. 1991. The "particle" flux: Origins and biological components. Prog. Oceanogr. **26**: 75–113. doi:10.1016/0079-6611(91)90007-9

Steinberg, D. K., C. A. Carlson, N. R. Bates, S. A. Goldthwait, L. P. Madin, and A. F. Michaels. 2000. Zooplankton vertical migration and the active transport of dissolved organic and inorganic carbon in the Sargasso Sea. Deep-Sea Res. Part I **47**: 137–158. doi:10.1016/S0967-0637(99)00052-7

Steinberg, D. K., J. S. Cope, S. E. Wilson, and T. Kobari. 2008*a*. A comparison of mesopelagic mesozooplankton community structure in the subtropical and subarctic North Pacific Ocean. Deep-Sea Res. Part II **55**: 1615–1635. doi:10.1016/j.dsr2.2008.04.025

Steinberg, D. K., B. A. S. Van Mooy, K. O. Buesseler, P. W. Boyd, T. Kobari, and D. M. Karl. 2008*b*. Bacterial vs. zooplankton control of sinking particle flux in the ocean's twilight zone. Limnol. Oceanogr. **53**: 1327–1338. doi:10.4319/lo.2008.53.4.1327

Steinberg, D. K., and M. R. Landry. 2017. Zooplankton and the ocean carbon cycle. Ann. Rev. Mar. Sci. **9**: 413–444. doi:10.1146/annurev-marine-010814-015924

Straile, D. 1997. Gross growth efficiencies of protozoan and metazoan zooplankton and their dependence on food concentration, predator-prey weight ratio, and taxonomic group. Limnol. Oceanogr. **42**: 1375–1385. doi:10.4319/lo.1997.42.6.1375

Stukel, M. R., M. R. Landry, C. R. Benitez-Nelson, and R. Goericke. 2011. Trophic cycling and carbon export relationships in the California Current Ecosystem. Limnol. Oceanogr. **56**: 1866–1878. doi:10.4319/lo.2011.56.5.1866

Stukel, M. R., M. D. Ohman, C. R. Benitez-Nelson, and M. R. Landry. 2013. Contributions of mesozooplankton to vertical carbon export in a coastal upwelling system. Mar. Ecol. Prog. Ser. **491**: 47–65. doi:10.3354/meps10453

Stukel, M. R., M. Kahru, C. R. Benitez-Nelson, M. Décima, R. Goericke, M. R. Landry, and M. D. Ohman. 2015. Using Lagrangian-based process studies to test satellite algorithms of vertical carbon flux in the eastern North Pacific Ocean. J. Geophys. Res. Oceans **120**: 7208–7222. doi:10.1002/2015JC011264

Stukel, M. R., and others. 2017. Mesoscale Ocean fronts enhance carbon export due to gravitational sinking and subduction. Proc. Natl. Acad. Sci. USA **114**: 1252–1257. doi:10.1073/pnas.1609435114

Stukel, M. R., H. Song, R. Goericke, and A. J. Miller. 2018. The role of subduction and gravitational sinking in particle export, carbon sequestration, and the remineralization length scale in the California Current Ecosystem. Limnol. Oceanogr. **63**: 363–383. doi:10.1002/lno.10636

Suzuki, N., and F. Not. 2015. Biology and ecology of radiolaria, p. 179–222. *In* Marine protists. Springer.

Takahashi, K., and S. Honjo. 1981. Vertical flux of Radiolaria: A taxon-quantitative sediment trap study from the western tropical Atlantic. Micropaleontology **27**: 140–190. doi:10.2307/1485284

Taylor, A. G., R. Goericke, M. R. Landry, K. E. Selph, D. A. Wick, and M. J. Roadman. 2012. Sharp gradients in phytoplankton community structure across a frontal zone in the California current ecosystem. J. Plankton Res. **34**: 778–789. doi:10.1093/plankt/fbs036

Visser, A. W., and U. H. Thygesen. 2003. Random motility of plankton: Diffusive and aggregative contributions. J. Plankton Res. **25**: 1157–1168. doi:10.1093/plankt/25.9.1157

Acknowledgments

We are immensely grateful to the Captains and crews of the R.V. *Melville* and R.V. *Sikuliaq* and to our many collaborators in the CCE LTER program who have enabled us to collect this dataset across many cruises and at times challenging conditions. We are also grateful to M. Picheral for his help with UVP5 data. Data used in this study are available on the CCE LTER Datazoo repository: https://oceaninformatics.ucsd.edu/datazoo/catalogs/ccelter/datasets. This work was funded by NSF grants to the CCE LTER Program: OCE-0417616, OCE-1026607, OCE-1637632, and OCE-1614359.

Conflict of Interest

None declared.

Submitted 27 March 2018
Revised 24 April 2018
Accepted 23 May 2018

Associate editor: Susanne Menden-Deuer